processes

MDPI

Article

Performance Evaluation of the Ultrasonic Humidification Process for HDH Desalination Applications

Aurora C. Duran, Keny Parisheck and Mostafa H. Sharqawy *

College of Engineering, University of Guelph, Guelph, ON N1G 2W1, Canada
* Correspondence: melsharq@uoguelph.ca; Tel.: +1-(519)-824-4120 (ext. 58973)

Abstract

Water scarcity remains a critical global challenge, driving the need for efficient small-scale desalination technologies. This study presents experimental research on the performance evaluation of an innovative ultrasonic humidifier designed for the humidification–dehumidification (HDH) desalination process. A prototype was designed, incorporating a 1.7 MHz piezoelectric transducer. The efficiency of the humidifier, the vapor production rate, and the specific energy consumption were evaluated based on two operating parameters: water temperature, ranging from 30 °C to 60 °C, and airflow rate, ranging from 20 to 120 L/min. The results show that humidification efficiency increases with airflow rate, reaching values above 95% at a temperature of 60 °C, with an airflow rate of 60 L/min, decreasing slightly at higher flow rates. The system demonstrated optimal performance at 60–80 L/min, balancing high efficiency and vapor production with moderate energy demand. These findings demonstrate that ultrasonic humidification is a viable alternative, especially in decentralized applications, due to its low thermal energy requirements, compact design, and adaptability to intermittent renewable energy sources.

Keywords: ultrasonic humidification; desalination; humidification–dehumidification; ultrasonic transducer; vapor production; humidity ratio

check for updates

Academic Editor: Youguo Yan

Received: 7 August 2025
Revised: 10 October 2025
Accepted: 16 October 2025
Published: 21 October 2025

Citation: Duran, A.C.; Parisheck, K.; Sharqawy, M.H. Performance Evaluation of the Ultrasonic Humidification Process for HDH Desalination Applications. *Processes* **2025**, *13*, 3374. https://doi.org/10.3390/pr13103374

Copyright: © 2025 by the authors. Licensee MDPI, Basel, Switzerland. This article is an open access article distributed under the terms and conditions of the Creative Commons Attribution (CC BY) license (https://creativecommons.org/licenses/by/4.0/).

1. Introduction

Inadequate water management, population growth, and climate change have all exacerbated the already existing problem of water scarcity. Fresh water resources are very limited, and are decreasing due to climate conditions, over exploitation, and aquatic systems pollution. As most of the world's water resources are in the form of ocean saltwater, representing 97.5% of water on Earth [1], finding an appropriate functional solution for desalination has become imperative and a priority. Clean and freshwater resources remain non-negotiable when it comes to human well-being and sustainable development. Efforts include the exploration of diverse desalination methods that can address the challenge at hand with environmental and monetary efficiency. Desalination separates dissolved salt substances in sea or brackish water to obtain pure drinking water. Existing large scale desalination methods can be divided into two main groups: phase-change processes and single-phase processes. The first category is represented by thermal processes, such as Multistage Flash (MSF), Multi-Effect Distillation (MED) and Vapor Compression (VC), while the second category is represented by membrane processes, such as Reverse Osmosis (RO), Nanofiltration (NF) and Electrodialysis (ED). While all these methods are energy-intensive, the specific energy requirements of each one vary significantly. Additionally, the use of renewable energy sources, such as waste heat recovery, and energy-efficient designs,

are both variables that affect the environmental impact and overall energy consumption of these desalination processes [2].

Desalination has become an indispensable technology for producing fresh water by removing dissolved salts from seawater and brackish water sources [3]. Conventional large-scale desalination methods are generally classified into two main categories: thermal-based (phase-change) processes and membrane-based (single-phase) processes [2]. Thermal desalination technologies, such as Multi-Stage Flash (MSF) and Multi-Effect Distillation (MED), involve heating saline water to produce a vapor, which is then condensed to yield fresh water [4]. These processes are energy-intensive but remain important in regions with access to low-cost thermal energy [5]. In contrast, membrane processes, particularly Reverse Osmosis (RO), utilize semi-permeable membranes to separate salts under high pressure, and have dominated new installations due to their lower specific energy consumption compared to thermal methods [6].

Nevertheless, desalination remains an energy-demanding process overall. The specific energy consumption varies significantly: MSF typically requires 15–25 kWh/m^3 while modern RO plants consume 3–5 kWh/m^3 for seawater desalination [7,8]. This high energy demand underscores the importance of integrating renewable energy sources and optimizing system designs to improve sustainability and reduce operational costs [9,10].

These larger-scale desalination systems provide mass freshwater production, and subsequently require extensive resources and investments and so are predominantly used in large cities. In comparison, humidification–dehumidification (HDH) systems can be utilized as a less demanding system that can be applied in medium to small coastal regions. HDH systems have the benefit of their simpler design and easier operating conditions, such as low working temperatures, less electricity, and less space consumption. Their low thermal energy requirement easily allows for the application of renewable energy, such as solar, geothermal, or waste energy, providing a more sustainable and practical solution to water desalination because of their smaller scale [3].

HDH systems are built to mimic the natural evaporation cycle. Freshwater is separated from impurities by converting saltwater into atomized water particles (humidification) and then condensed into freshwater (dehumidification). During the humidification process, the saltwater is made into small saltwater droplets to allow for a high overall surface area for the air and water to interact. Once the saltwater droplet gains enough energy it can break its bonds and become a small pure water particle that can be absorbed by air; this is evaporation.

Any HDH system can be broken down into 3 main components: the humidifier, heater, and dehumidifier. This paper focuses on the humidification process. Different methods of desalination using a HDH system have been investigated, with varying heating and humidification methods. There are numerous heating methods that can be employed; however, the most common include solar, battery, and electricity. These heating methods are coupled with different humidification methods, such as in an investigation by Alrbai et al. [11] where heated water was sprayed using a fogging nozzle to generate tiny saltwater droplets and that evaporated with the introduction of air. Another experiment conducted by Eder et al. [12] used a bubble column humidifier; this technique created small water bubbles that amplified the surface contact area for the air to gain high humidity. Lastly, another instance of a HDH system, by Elsharqawy et al. [13], included pushing heated air through saltwater-concentrated packing beds, and as air passed through each bed, the air picked up more moisture and eventually became saturated with water droplets [13].

This paper centers on novel ultrasonic humidification techniques. The adoption of ultrasonic humidifiers, an innovative humidification method, can significantly enhance

HDH systems. This technology operates at low temperatures, which lowers energy demand without compromising humidification speed, thereby improving both sustainability and financial feasibility. Previous research on ultrasonic HDH systems explored replacing existing humidification devices in HDH systems with ultrasonic humidifiers available in the market.

The utilization of HDH techniques to enhance other desalination processes has been studied to analyze the overall efficiency impact. El-Said and Abdelaziz [14] studied the influence of high frequency ultrasound atomizers (HFU) on the performance of a solar still (SS), garnering a productivity and thermal efficiency increase alongside a reduction in costs when using this hybrid system. Thermal efficiency was closely linked to the number of atomizers and water height; it decreased with the increment of water height and with the increment of atomizers. The continuous operation vs. pulsating operation was studied, obtaining a better performance by 72% using 25 min on-and-off cycles. More research from El-Said et al. [15] studied the impact of hot air stream flow on a hybrid solar desalination system, and the results showed that when primary operational factors (water height and atomizer number) remained fixed, variation in air mass flow rate strongly influenced the system's performance, with the best results being achieved using six atomizers in a 77 cm $\times$ 77 cm tank with 1 cm water height.

In another investigation, Shehata et al. [16] performed a two-stage humidification process, where the saltwater spraying technique was used in conjunction with ultrasonic foggers. Saltwater was first heated using a solar collector and then sprayed from above in the humidification chamber. Hot air was blown horizontal to the spray and pushed the saltwater vapor though five ultrasonic foggers. These foggers were added to enhance the humification system performance. Ultimately, they found that the ultrasonic humidifier improved their daily production by 9.3% and increased maximum air mass flow rate by 14.6%.

Furthermore, a similar investigation by Tourab et al. [17] also demonstrated enhanced humidification effectiveness when using an ultrasonic water atomizer with an array of ten piezoelectric transducers, combined with the traditional spraying atomization. They also concluded that a 20–30 min operating time was optimal for reaching a steady state. The maximum humidification effectiveness reached was 94.9%, which was a 25.2% increase compared to without the ultrasonic atomizer, further displaying the powerful and efficient humidification ability of ultrasonic foggers.

Abed et al. [18] studied a hybrid system of a single-slope solar still unit with phase change material (PCM) capsules and a high frequency ultrasonic vaporizer. The results indicated that high water productivity was achieved with a dual system of an external solar water heater and a HFU vaporizer, about 415%. Findings regarding the intermittent functioning of the ultrasonic vaporizer showed that a higher thermal efficiency was reached within 30 min of the operation time. Overall, the experimental results showed that the HFU vaporizer had a notable effect on thermal performance and productivity.

To measure the adsorption isotherms and kinetics of water vapor onto porous materials, Ehab et al. [19] used an ultrasonic wave device submerged in 5 cm water depth for continuous working to generate vapor inside a sample chamber. Temperature and relative humidity sensors were used to measure the parameters inside of the chamber. This study found that the addition of the ultrasonic device allowed for a greater vapor flowrate and operating pressure control and led to a significantly decreasing the apparatus capital cost.

This study advances the understanding of ultrasonic humidification in humidification–dehumidification (HDH) desalination systems. An experimental prototype was developed and tested under a range of operating conditions. Using thermodynamic analysis and key performance metrics—including air mass flow rate, humidification capacity, process

efficiency, and specific energy consumption—the system's behavior was evaluated, and optimal operational parameters were identified.

2. Materials and Methods

2.1. Experimental Setup

An experimental design and procedure were conducted to complete a series of tests on the effectiveness of the ultrasonic humidification device. The ultrasonic humidification device model and cross-section can be seen in Figure 1. This device can be broken down into three separate components: the inside chamber, outside chamber and mixing section.

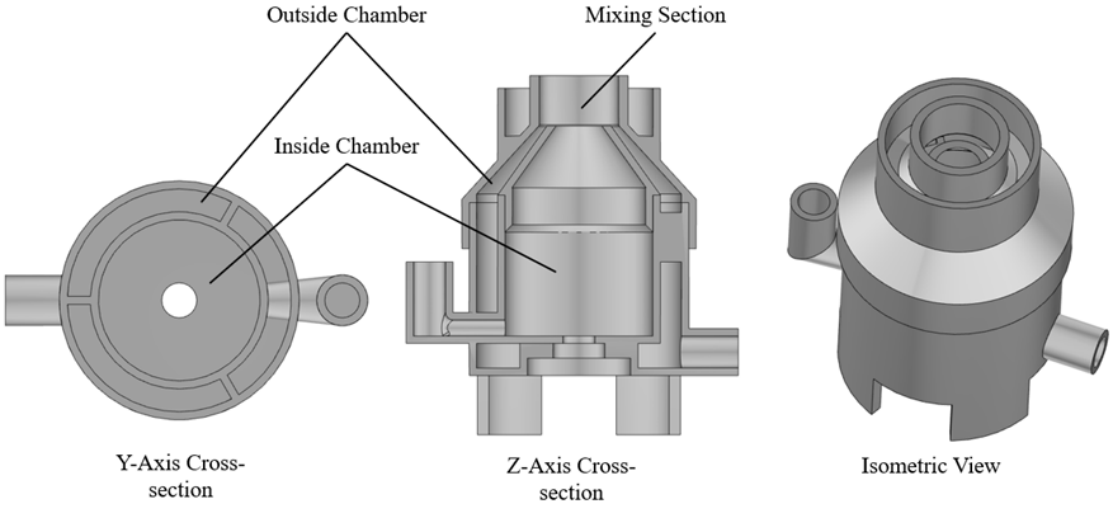


Figure 1. Cross-section and 3D model of main ultrasonic humidifier part.

The inside chamber is filled with a layer of heated water. Heating the water increases the kinetic energy and subsequently the air's ability to absorb more water particles, thereby increasing the system's efficiency. The ultrasonic transducer sits below the layer of water and is fixed to the bottom of the inner chamber. This ceramic piezoelectric transducer takes electricity and converts it into mechanical oscillations that vibrate at ultrasonic frequencies. These vibrations generate numerous small cavitations within the water, causing atomized saltwater droplets to be emitted in the air as saltwater vapor. The mixing section is where the opening of the inside and outside chamber converges in a conical shape. This allows the air flowing though the outside section to mix with the atomized saltwater by employing the Venturi effect. This effect pushes the generated fog out at a greater speed because of the significant drop in pressure at the opening. This later allows for a greater mixing of the air and fog in the PVC pipe, thus increasing the evaporation rate. The relevant dimensions of the humidification device are in Table 1.

Table 1. Dimensions of system components.

	Diameter	Height	Displacement from Inside Chamber
Inside chamber	60 mm	60 mm	-
Outside chamber	83 mm	67 mm	8.5 mm
Wall thickness	3 mm	-	-
Mixing section diameter	32.5 mm	-	-
Transparent PVC pipe length	400 mm	-	-
Ultrasonic transducer diameter	20 mm	-	-

The full schematic of the experimental setup can be seen in Figure 2 and a photo of the setup is shown in Figure 3. It consists of an ultrasonic humidifier with a water inlet, an air inlet, and a humidified air outlet. An SHT35 sensor (manufactured by Sensirion AG, Stäfa, Switzerland), measuring inlet temperature and humidity, is placed in the air inlet. The water temperature is regulated with a temperature sensor and a 50 W electric cartridge heater. A 1.7 MHz ultrasonic piezoelectric transducer is secured under a hole at the bottom of the inside chamber. After the transducer atomizes the heated saltwater, it evaporates within a clear 40 cm PVC pipe. Another SHT35 temperature and humidity sensor is placed at the exit of the PVC pipe (humidified air outlet). The airflow was measured using an Omega rotameter, equipped with a fine needle valve for precise flow rate control. The instrument had a measurement range of 0–150 L/min. Although no significant scaling or fouling was observed during the 30 min tests due to the short duration, long-term operation would likely require anti-fouling measures (e.g., periodic cleaning and pre-treatment) to maintain transducer performance. Future work should evaluate fouling effects over extended periods.

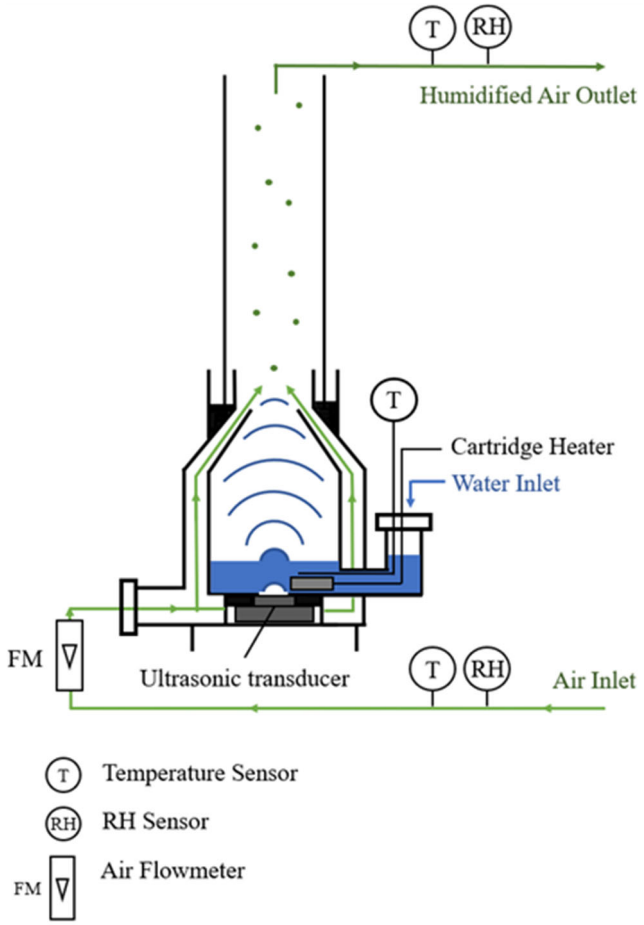


Figure 2. Ultrasonic humidifier schematic.

The experiment tests two changing variables: the temperature of inlet water and the inlet airflow rate. The measured dependent variables are the inlet air temperature, inlet air humidity, outlet air temperature, and outlet air humidity. The water height was maintained at 2 cm during the experiment. The 2 cm height reduces the risk of the water quickly drying out and exposing the cartridge heater to air, as is seen with a 1 cm water height.



Figure 3. Picture of experimental setup.

The testing consisted of maintaining the inlet water temperature at 60 °C, and then at 45 °C, 30 °C, and finally, 35 °C, while changing the inlet airflow rate. Eleven tests were performed every 10 L/min within a 20–120 L/min range. Each test duration lasted 30 min, as this was proven in previous studies to be the optimal time for reaching a steady state [14,17]. At 5 min intervals, water levels were measured and refilled, depending on the amount of water lost. Using Arduino data logging software V 4.1.0, the temperature and humidity of the inlet and outlet were measured, using the two humidity and temperature sensors. This data was then graphed and analyzed. The temperature range (30–60 °C) was selected to represent realistic conditions achievable by low-grade thermal sources (e.g., solar, thermal and waste heat). The airflow range (20–120 L/min) was chosen to evaluate system performance from near-static conditions up to the operational limit of the transducer, covering potential real-world applications, from small-scale standalone units to larger modular systems.

2.2. Mathematical Model

This model is a system consisting of an ultrasonic humidification device, water heater, air inlet, water inlet, and a humidified air outlet, in which the steady state of humidity and temperature is measured at the air inlet and outlet. The objective of this model is to measure the system's performance and efficiency under different working conditions (i.e., changing flow rate and water temperature). This model assumes that:

- The water temperature is fixed at the specified temperature during testing.
- The airflow rate is constant at the specific airflow rate being tested.
- The humidity of the room has no effect on the performance of the device.
- The heat from the water temperature has a negligible effect on the air temperature.

The air mass flow rate equation determines the mass of air entering the system over time and is given by Equation (1):

$$\dot{m}_a = \dot{v}_a \times \rho_a \tag{1}$$

where $\dot{v}_a$ is the inlet airflow rate converted from L/m to m^3/s. This is multiplied by the density of air, ρ_a.

The humidification capacity equation calculates the mass of vapor produced at the air outlet over time and is given by Equation (2):

$$\dot{m}_V = \dot{m}_a \, (\omega_{out} - \omega_{in}) \tag{2}$$

where ω_{out} and ω_{in} are the humidity ratios at the outlet and inlet, respectively, and $\dot{m}_a$ is the air mass flow rate determined in Equation (1). For graphing purposes this is converted from kg/s to kg/h.

The heat transfer rate to the air is calculated using Equation (3):

$$\dot{Q} = \dot{m}_a(h_{out} - \ h_{in}) \tag{3}$$

where h_{out} and h_{in} are the enthalpy of moist air at the outlet and inlet, respectively, and $\dot{m}_a$ is the air mass flow rate determined in Equation (1).

Using the values calculated in Equations (2) and (3), the humidifier specific energy consumption can be calculated using Equation (4):

$$SEC_H = \dot{Q}/\dot{m}_v \tag{4}$$

where $\dot{Q}$ is the heat transfer rate and $\dot{m}_v$ is the humidification capacity in the outlet air.

The humidification efficiency evaluates the device's effectiveness at humidifying vapor by dividing the actual experimental humidity ratio by the theoretical maximum humidity ratio ω_{in}. This is given by Equation (5):

$$\eta_H = \frac{\omega_{out} - \omega_{in}}{\omega_{max} - \omega_{in}} \tag{5}$$

where ω_{out} and ω_{in} represents the measured humidity ratio out and in, respectively. In addition, ω_{max} is the humidity ratio when RH = 100% at the outlet air temperature.

2.3. Uncertainty Analysis

An uncertainty analysis was conducted to evaluate the reliability and accuracy of the experimental measurements used in the performance assessment of the ultrasonic humidifier. The primary sources of uncertainty were associated with the sensors and instruments used to record the temperature, relative humidity, water level, and airflow rate. Temperature and humidity measurements were obtained using SHT35 digital sensors, which have an accuracy of ± 0.1 °C for temperature and $\pm 1.5\%$ RH for humidity. These sensors were placed at both the inlet and outlet of the air stream. The uncertainty in airflow rate was determined using a calibrated flowmeter, with a tolerance of $\pm 2\%$ of full scale. The water level in the humidification chamber was measured manually, with a resolution of 1 mm.

3. Results and Discussion

This section presents and analyzes the experimental results obtained from the operation of the ultrasonic humidifier under different water temperatures and airflow rates. The main performance indicators evaluated were humidification efficiency, water vapor

production rate, and specific energy consumption, which were calculated from temperature and relative humidity data measured at the inlet and outlet of the humidifier. The impact of the airflow rate and water temperature on the system's performance were assessed through a series of parametric tests. These results are discussed to identify the optimal operating conditions for maximizing the system's efficiency and vapor output, as well as to understand the thermodynamic behavior of the humidification process under varying conditions.

Figures 4–7 show the humidifier efficiency variation with airflow rate and water temperature. Figure 4 illustrates the variation in the humidification efficiency with airflow rate, at a water temperature of 30 °C. The efficiency increases markedly with airflow, reaching a peak between 60 and 80 L/min, due to a greater mass transfer driving force as more dry air becomes available to absorb vapor [10]. Beyond this optimum, efficiency gradually declines because the residence time of air in the chamber decreases, limiting vapor absorption. This trend aligns with findings by Tourab et al. [17], who observed a similar peak-then-decline pattern and attributed the optimal point to maximized mass transfer, with the subsequent decline resulting from insufficient contact time at higher flows.

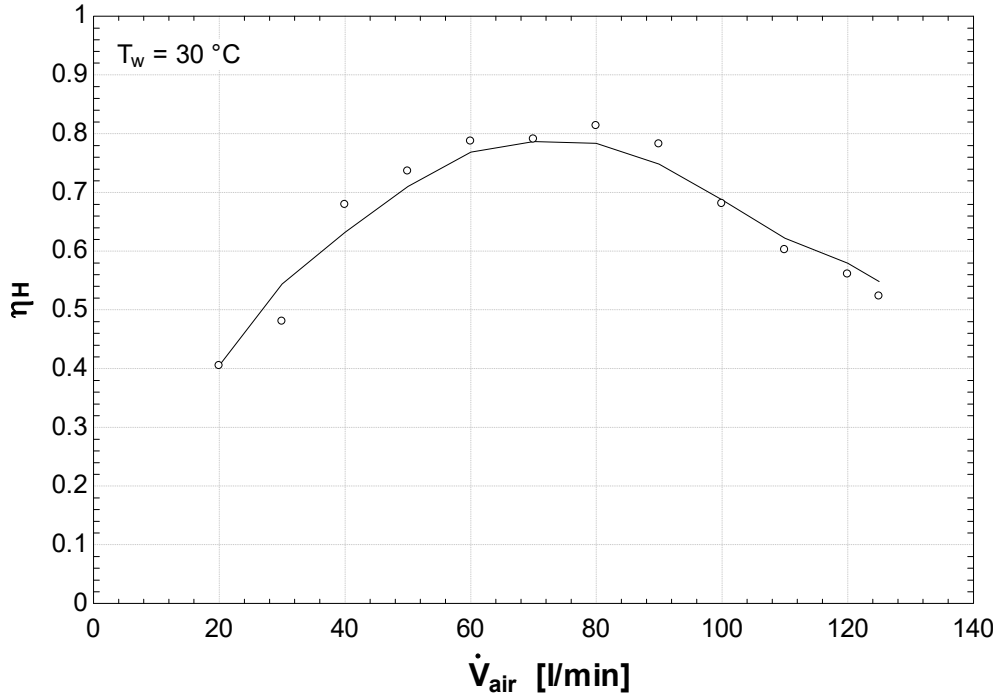


Figure 4. Humidifier efficiency variation with the airflow rate, at water temperature of 30 °C.

Figure 5 presents a test with a water temperature of 35 °C. The humidification efficiency behavior shows an increasing trend with the increase in airflow, reaching values close to 90%. This progressive increase is due to a greater amount of dry air available to absorb the vapor generated by the ultrasonic humidifier. Efficiency stabilizes in a flow range between approximately 70 and 100 L/min, indicating that the system is operating under optimal mass transfer conditions. However, when the airflow exceeds 80 L/min, a slight decrease in efficiency is observed, likely due to the reduced air–water contact time at higher velocities, which limits complete saturation. This trend aligns with findings by El-Said et al. [14].

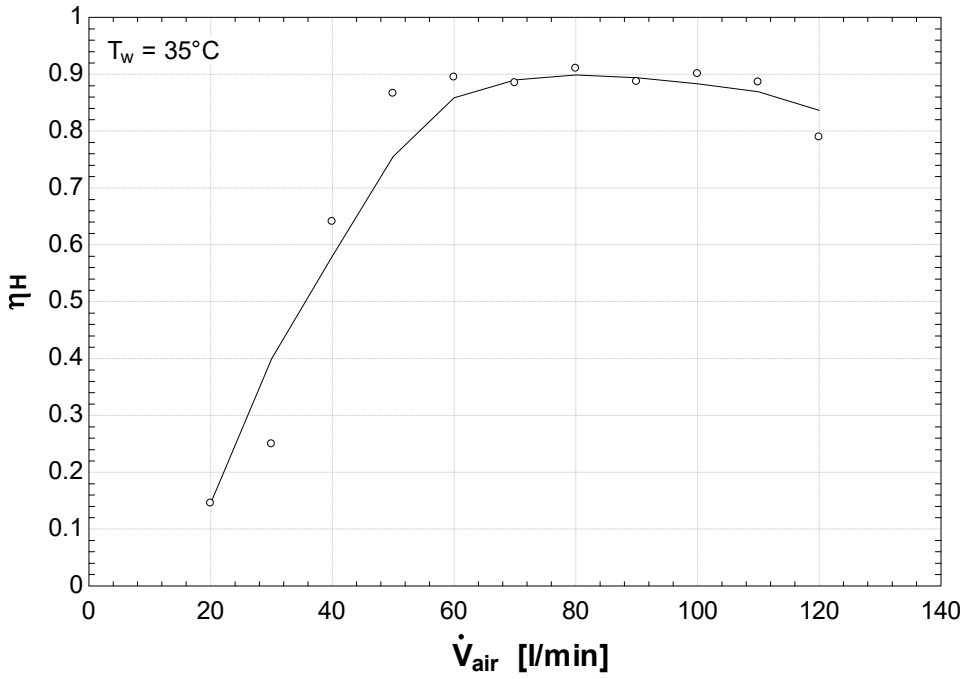


Figure 5. Humidifier efficiency variation with the airflow rate, at water temperature of 35 °C.

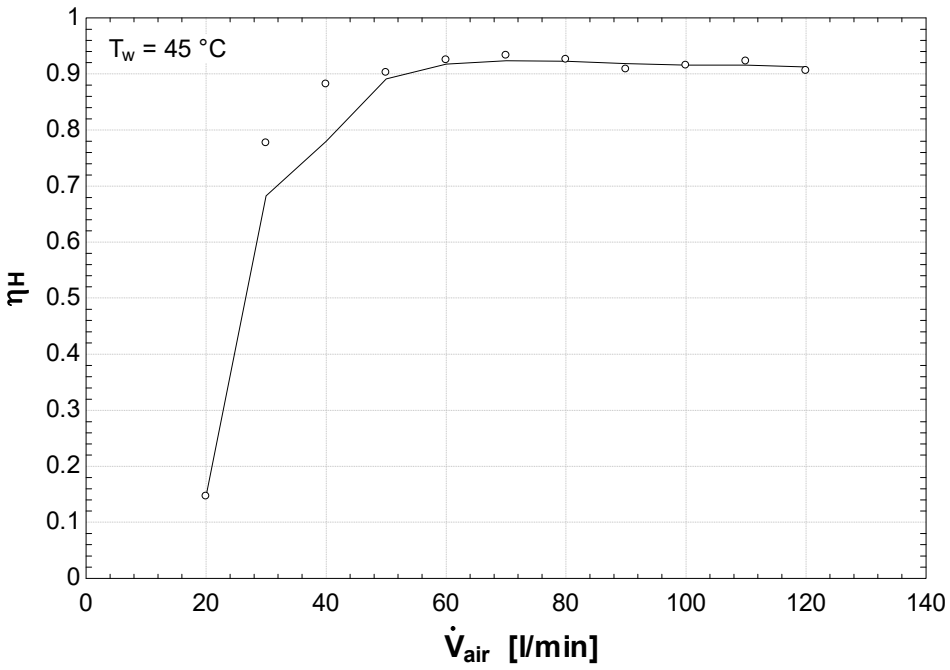


Figure 6. Humidifier efficiency variation with the airflow rate, at water temperature of 45 °C.

Figure 6 illustrates the humidification efficiency variation with airflow rate, at a water temperature of 45 °C. The efficiency shows a rapid increase at low flow rates, reaching above 90% once the flow exceeds approximately 50 L/min. This sharp improvement indicates an enhanced mass transfer as more dry air becomes available to absorb the atomized droplets. The stabilization of the efficiency above 90% across a wide flow range (50–110 L/min) suggests a well-balanced interaction between the ultrasonic transducer's droplet generation rate and the air's moisture absorption capacity. This equilibrium phenomenon aligns with findings by Shehata et al. [16], who observed that ultrasonic foggers achieve their maximum performance when atomization rates match the air's vapor-carrying capacity, enabling stable high-efficiency operation across varying airflow conditions.

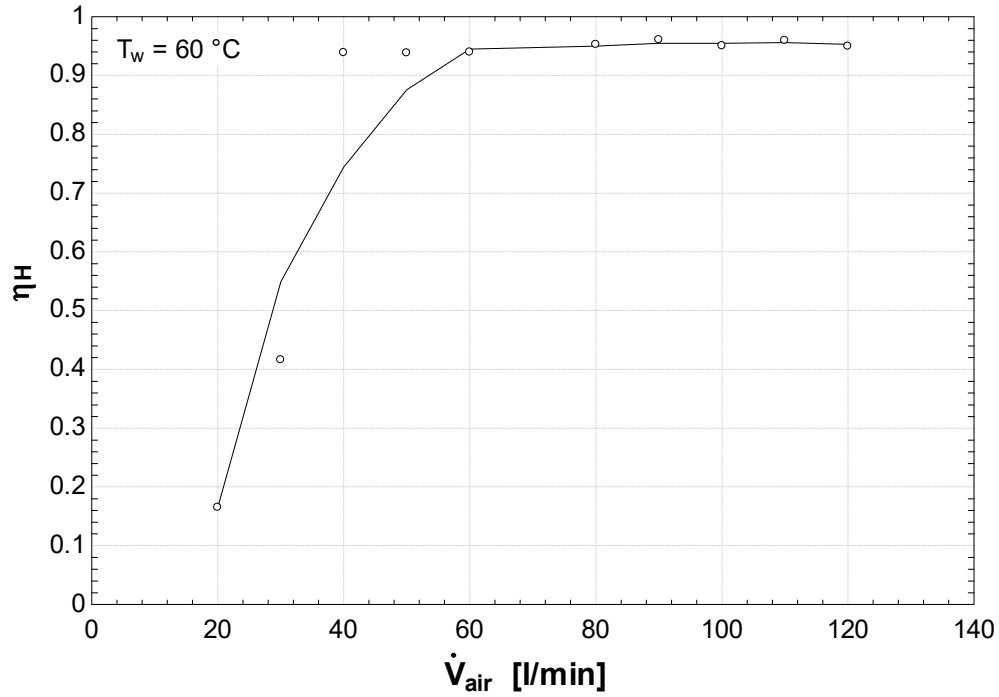


Figure 7. Humidifier efficiency variation with the airflow rate, at water temperature of 60 °C.

Figure 7 demonstrates the system's outstanding humidification performance, at 60 °C, with its efficiency exceeding 95% at approximately 60 L/min and maintaining this high level consistently up to 120 L/min. This behavior confirms that the greater thermal energy available at this elevated temperature significantly enhances vaporization and facilitates rapid air saturation. The sustained high efficiency across the entire flow range, without the decline at high flow rates observed at lower temperatures, indicates that the increased water temperature overcomes the limitation of the reduced residence time at high flow rates. The increase in water temperature reduces surface tension and enhances the droplet atomization and evaporation. This performance enhancement aligns with findings by El-Said and Abdelaziz [14], who reported that ultrasonic atomizers operating above 50 °C maintain near-saturation conditions even at elevated airflow rates, due to improved evaporation kinetics and reduced water surface tension.

Figures 8–11 illustrate humidification water vapor production, analyzing the relationship between the water vapor production rate ($\dot{m}_v$) and the airflow rate, at different water temperatures. The objective is to understand how the amount of vapor generated by the ultrasonic humidifier varies as thermal and flow conditions change.

Experimental evaluations were carried out at four water temperatures: 30 °C, 35 °C, 45 °C, and 60 °C. In each case, the airflow rate was gradually increased from 20 to 125 L/min, and the mass of vapor produced per hour was measured. These tests allow for the identification of the system's dynamic behavior and its vapor-generation capacity under different levels of thermal energy input.

The resulting graphs show a growing trend in ($\dot{m}_v$) with increasing airflow rate, though the slope and saturation point vary depending on the water temperature. This analysis is key to determining the effective capacity of the system, as well as its energy adaptability under varying operational conditions.

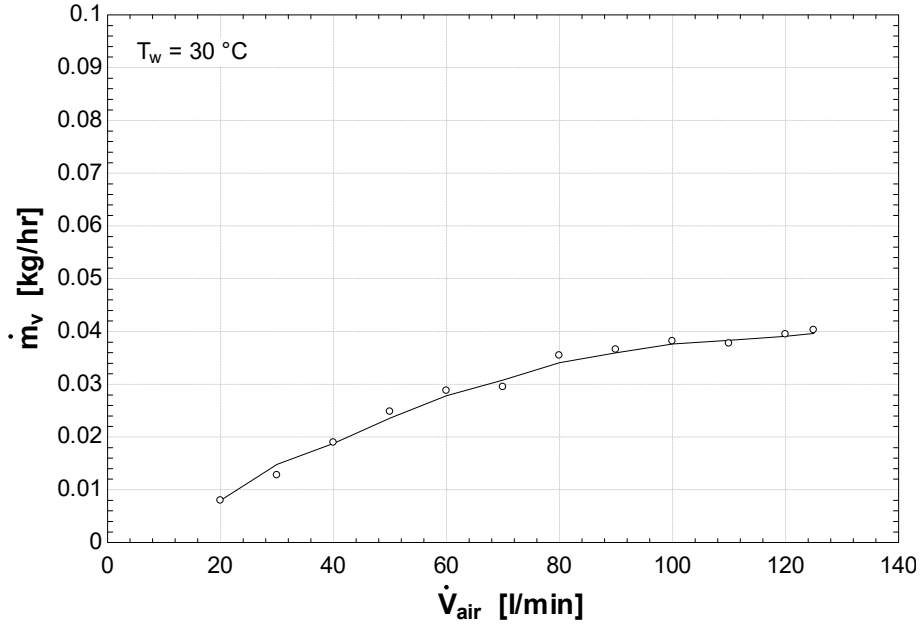


Figure 8. Humidification water vapor production vs. airflow rate, at 30 °C.

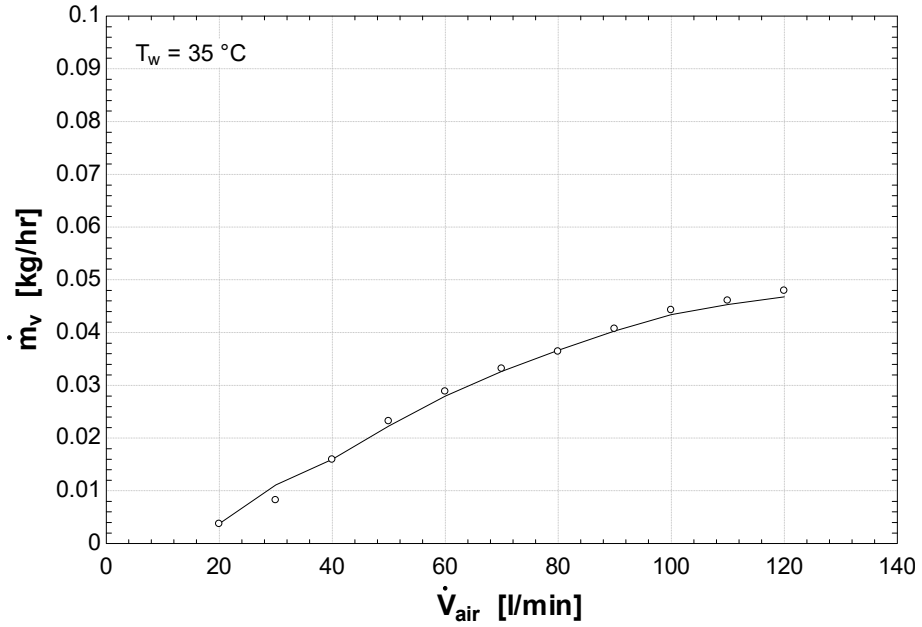


Figure 9. Humidification water vapor production vs. airflow rate, at 35 °C.

Figure 8 indicates a positive correlation between airflow and water vapor production at 30 °C. As airflow increases, a greater volume of dry air passes through the humidifier, increasing its capacity to transport vaporized water molecules. Consequently, the vapor production rate shows a progressive increase across the measured range. However, the curve reveals a decreasing rate of increase as the airflow exceeds 80 L/min, suggesting a trend toward saturation. This behavior can be attributed to the limited energy input at 30 °C, which restricts the rate of vapor generation despite the availability of additional airflow. This thermal limitation phenomenon aligns with findings by Abed et al. [18], who observed that in ultrasonic humidification systems, vapor production becomes constrained by available thermal energy rather than airflow capacity when operating at lower temperatures. As a result, the system's ability to further increase its vapor production is limited by

thermal conditions rather than by flow dynamics, which is consistent with mass transfer principles in thermally limited evaporation processes.

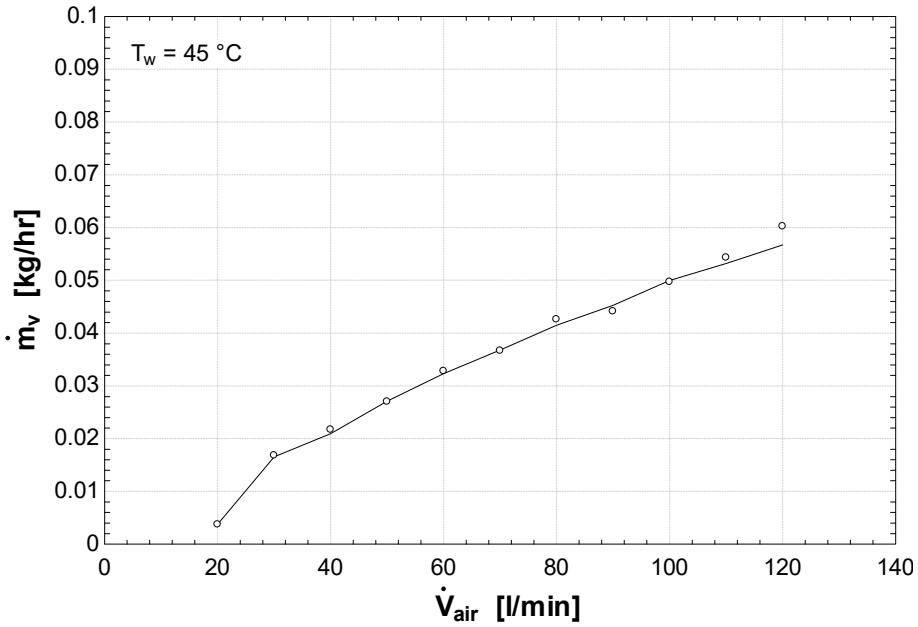


Figure 10. Humidification water vapor production vs. airflow rate, at 45 °C.

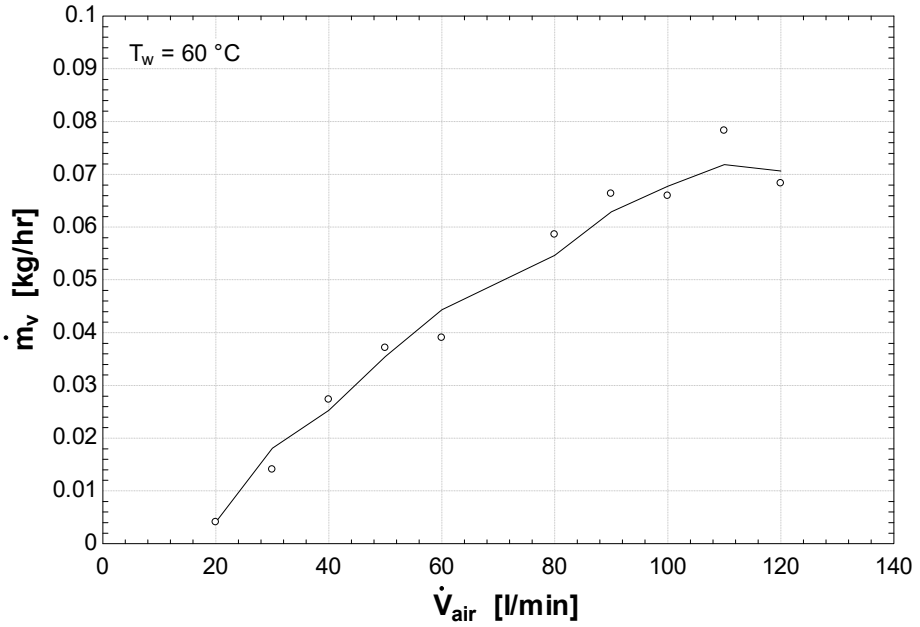


Figure 11. Humidification water vapor production vs. airflow rate, at 60 °C.

Figure 9 shows the water vapor production rate at 35 °C, reaching a maximum value of approximately 0.05 kg/h. This represents a significant increase compared to the maximum of 0.04 kg/h observed at 30 °C (Figure 8), demonstrating the positive effect of elevated temperature on vapor generation. The higher thermal energy, at 35 °C, provides more energy to overcome the water's latent heat of vaporization, resulting in enhanced atomization efficiency. This temperature-driven performance gain corroborates studies by Shehata et al. [16], where thermal augmentation in ultrasonic atomizers was linked to improved nebulization efficacy through decreased cohesive forces and accelerated droplet nucleation. The data confirm that a minimal temperature rise can significantly elevate vapor production in HDH applications.

Figure 10 exhibits a nearly linear relationship between water vapor production and airflow rate at 45 °C, indicating that the system maintains efficient humidification across the tested flow range. This linear trend suggests that the thermal energy at 45 °C provides a sufficient driving force for vaporization, without reaching saturation limits. The consistent slope demonstrates that vapor generation keeps pace with increasing air capacity to transport moisture. This behavior aligns with findings by El-Said et al. [15], who observed linear vapor production trends in hybrid solar ultrasonic systems operating in the 40–50 °C range, attributing this to the optimal balance between thermal input and ultrasonic atomization efficiency. The results confirm that 45 °C represents an operational sweet spot, where thermal and flow parameters synergistically enhance performance.

Figure 11 demonstrates the optimal performance of the ultrasonic humidifier at 60 °C, showing a pronounced increase in water vapor production from 20 to 110 L/min. This robust upward trend reflects the enhanced evaporation kinetics, where elevated thermal energy reduces water surface tension and facilitates molecular bond dissociation, thereby increasing vaporization rates. The slight performance decline at 125 L/min suggests approaching the system's maximum vapor transport capacity, where residence time limitations begin to affect saturation efficiency.

This performance characteristic corresponds with reports by Shehata et al. [16] which indicate that ultrasonic HDH systems reach their maximum vapor output under combined high thermal energy (55–65 °C) and moderated airflow conditions, and establish an optimal regime for phase transition efficiency. The present results corroborate 60 °C as the most effective thermal level for maximizing vapor generation in ultrasonic humidification process.

To comprehensively evaluate the energy performance of the ultrasonic humidifier, the specific energy consumption (SE_h) was assessed. SE_h is defined as the amount of thermal energy required to produce one kilogram of water vapor, and serves as a critical metric for determining the energy efficiency of the system under different operating conditions. By analyzing how SE_h changes with different airflow rates at fixed water temperatures, valuable conclusions can be drawn about the device's optimal operating range.

Figures 12–15 present the SE_h results for water temperatures of 30 °C, 35 °C, 45 °C, and 60 °C, highlighting the trade-offs between energy consumption and water vapor production. These findings are crucial for understanding the scalability and viability of ultrasonic humidification in HDH desalination systems, especially in resource-constrained environments where energy efficiency is paramount.

Figure 12 shows a decreasing trend in specific energy consumption (SE_h) with increasing airflow rate at 30 °C. The SE_h declines from approximately 0.60 kWh/kg at 20 L/min to 0.19 kWh/kg at 120 L/min, indicating a significant improvement in energy efficiency. This reduction occurs because the fixed thermal energy input is distributed across a greater mass of vapor produced as airflow increases. The stabilization of SE_h beyond 100 L/min suggests the system approaches its maximum vapor transport capacity under these thermal conditions. This behavior aligns with the thermodynamic principles governing energy efficiency in humidification processes, where increased mass flow rates enhance energy utilization by improving heat and mass transfer coefficients [3]. Similar trends have been observed in packed-bed humidification systems, where higher airflow rates reduce specific energy consumption until system limits are reached [13].

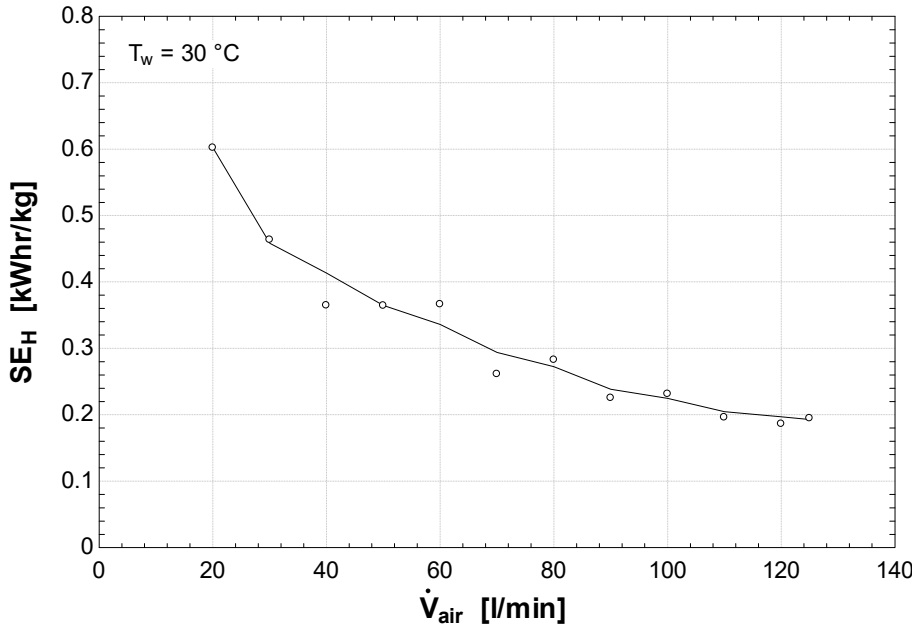


Figure 12. Specific energy consumption of the ultrasonic humidifier at 30 °C vs. airflow rate.

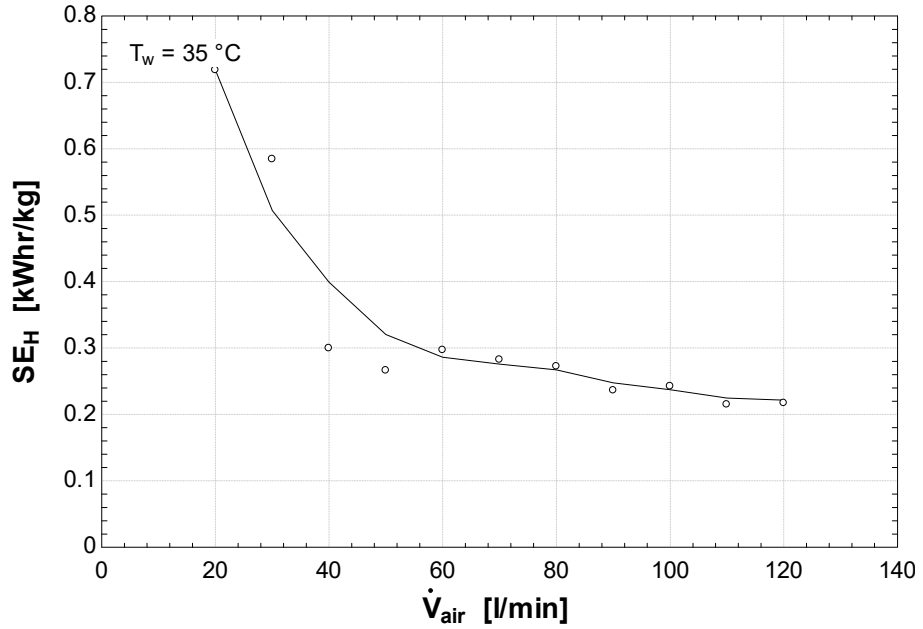


Figure 13. Specific energy consumption of the ultrasonic humidifier at 35 °C vs. airflow rate.

In Figure 13, the specific energy consumption (SE_h) continues to exhibit a decreasing trend as the airflow rate increases. Initially, the SE_h value is relatively high, around 0.72 kWh/kg at 20 L/min, indicating inefficient operation due to limited vapor generation. However, a substantial drop occurs between 30 L/min and 40 L/min, reducing SE_h to approximately 0.30 kWh/kg. This sharp decline reflects a significant improvement in energy efficiency, likely due to the enhanced vaporization at moderate flow rates. Beyond 40 L/min, SE_h continues to decline gradually, reaching a stable value close to 0.22 kWh/kg from 110 L/min onwards. This trend reinforces the importance of selecting appropriate airflow rates to minimize energy consumption, especially in low-temperature humidification systems. This behavior is consistent with thermodynamic principles governing air–water contact systems, where moderate flow rates typically optimize the trade-off between the residence time and transfer coefficients [3]. The observed efficiency transition around

30–40 L/min aligns with findings from packed-bed humidification studies [13], which report similar critical flow thresholds for energy optimization. The results underscore that selecting airflow rates above this critical threshold is essential for the efficient operation of low-temperature ultrasonic humidification systems.

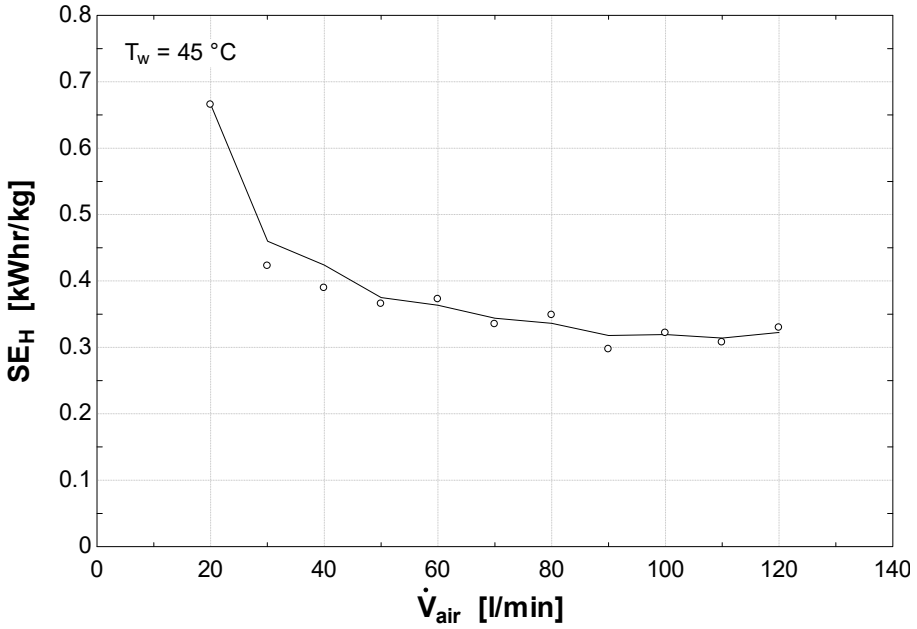


Figure 14. Specific energy consumption of the ultrasonic humidifier at 45 °C vs. airflow rate.

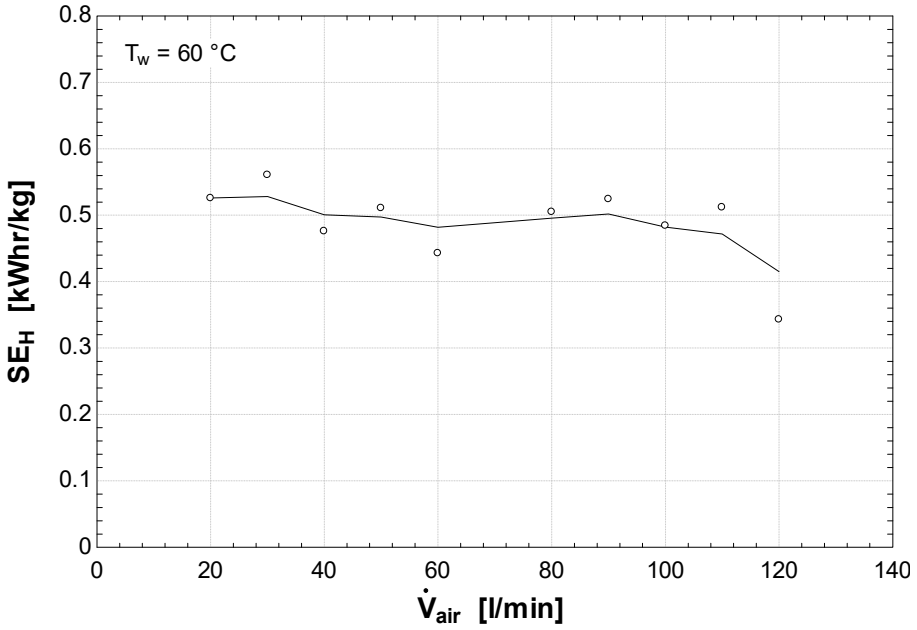


Figure 15. Specific energy consumption of the ultrasonic humidifier at 60 °C vs. airflow rate.

Figure 14 (SE_h) shows a similar pattern to that at lower temperatures, with a clear decrease as the airflow rate increases. Starting at a value of approximately 0.66 kWh/kg at 20 L/min, there is a marked reduction in SE_h, reaching around 0.38 kWh/kg at 40 L/min. This initial drop suggests a significant improvement in the energy efficiency of the ultrasonic humidifier, driven by the increased mass and heat transfer capacity. From that point on, the curve stabilizes with slight fluctuations, remaining in a range between 0.33 and 0.38 kWh/kg. This efficiency stabilization corresponds to previously reported

optimal ultrasonic operations near 45 °C, where thermal and atomization rates achieve equilibrium [14]. The invariant SE_h above 40 L/min confirms system reliability under variable flow conditions as an essential characteristic for renewable energy applications subject to airflow fluctuations.

Figure 15 reveals a distinct specific energy consumption (SE_h) profile at 60 °C, remaining nearly constant within 0.41–0.55 kWh/kg across the entire airflow range. This plateau indicates that the system has reached its fundamental efficiency limit, transitioning from thermally limited to transducer-limited operation. The behavior aligns with piezoelectric actuator studies [19], where performance plateaus occur when mechanical output saturates, despite increased input, and it corresponds to HDH optimization principles [3], where efficiency gains diminish beyond optimal temperature thresholds.

4. Conclusions

This study demonstrated that a single 1.7 MHz ultrasonic transducer with Venturi-shaped mixing achieves humidification efficiencies exceeding 95% across a broad airflow range (60–120 L/min), outperforming multi-transducer systems while maintaining a compact design. The optimal operational window was identified as 60 °C and 100–110 L/min, where vapor production reaches 0.08 kg/h—double the output at 30 °C. Key quantitative findings include the following: humidification efficiency peaks at 92–96% within 60–80 L/min airflow range, while specific energy consumption decreases from 0.72 kWh/kg at 20 L/min to 0.19–0.22 kWh/kg at high flows. At 60 °C, SE_h stabilizes at 0.41–0.55 kWh/kg, indicating energy efficiency limits under maximum atomization conditions.

The system achieves 25–30% higher vapor production per degree Celsius temperature increase, with the most significant gain (40%) occurring between 45 °C and 60 °C. These performance metrics, coupled with its low thermal requirements (30–60 °C), position ultrasonic humidification as a viable solution for small-scale HDH desalination.

Overall, the findings demonstrate that ultrasonic humidification within HDH configurations offers a viable alternative for small-scale desalination processes, with the potential for optimization through appropriate operational adjustments. Further studies are recommended, including economic analysis, long-term performance evaluation, and system scalability to assess its applicability in real-world water supply scenarios. The scale-up of this system would likely involve the modular replication of transducer units rather than increasing transducer size, due to the physical limitations of piezoelectric materials. Additionally, maintaining humidification efficiency at larger scales would require careful management of the air–water distribution and pressure drop across the system. Future work should focus on modular design approaches to facilitate field deployment, enhance scalability, and simplify maintenance, while also considering economic analysis and fouling mitigation.

Author Contributions: Conceptualization, M.H.S.; methodology, M.H.S.; software, A.C.D.; formal analysis, A.C.D.; investigation, A.C.D.; resources, M.H.S.; data curation, A.C.D.; writing—original draft preparation, A.C.D. and M.H.S.; writing—review and editing, M.H.S. and K.P.; visualization, K.P.; supervision, M.H.S.; project administration, M.H.S. All authors have read and agreed to the published version of the manuscript.

Funding: This research was funded by the Natural Sciences and Engineering Research Council of Canada (NSERC) Grant number 401366, and MITACS Globalink research internship.

Data Availability Statement: The original contributions presented in this study are included in the article. Further inquiries can be directed to the corresponding author.

Conflicts of Interest: The authors declare no conflicts of interest.

Abbreviations

h	specific enthalpy	$J \cdot kg^{-1}$
$\dot{m}$	mass flow rate	$kg \cdot s^{-1}$
$\dot{Q}$	heat transfer rate	W
RH	relative humidity	%
SEC	Specific Energy Consumption	$J \cdot kg^{-1}$ of vapor
T	Temperature	°C
$\dot{v}$	volume flow rate	$m^3 \cdot s^{-1}$
Greek Symbols		
η	efficiency	-
ρ	density	$kg \cdot m^{-3}$
ω	humidity ratio	$kg_{vapor}/kg_{dry\ air}$
Subscripts		
a	air	
in	inlet	
max	maximum	
out	outlet	
v	vapor	
w	water	

References

1. Al-Kharabsheh, S.; Goswami, D.Y. Analysis of an innovative water desalination system using low-grade solar heat. *Desalination* **2003**, *156*, 323–332. [CrossRef]
2. Karagiannis, I.C.; Soldatos, P.G. Water desalination cost literature: Review and assessment. *Desalination* **2008**, *223*, 448–456. [CrossRef]
3. Shannon, M.A.; Bohn, P.W.; Elimelech, M.; Georgiadis, J.G.; Marinas, B.J.; Mayes, A.M. Science and technology for water purification in the coming decades. *Nature* **2008**, *452*, 301–310. [CrossRef] [PubMed]
4. El-Dessouky, H.T.; Ettouney, H.M. *Fundamentals of Salt Water Desalination*, 1st ed.; Elsevier Science: Amsterdam, The Netherlands, 2002; ISBN 9780444508102.
5. Narayan, G.P.; Sharqawy, M.H.; Summers, E.K.; Lienhard V, J.H.; Zubair, S.M.; Antar, M.A. The potential of solar-driven humidification-dehumidification desalination for small-scale decentralized water production. *Renew. Sustain. Energy Rev.* **2010**, *14*, 1187–1201. [CrossRef]
6. Greenlee, L.F.; Lawler, D.F.; Freeman, B.D.; Marrot, B.; Moulin, P. Reverse osmosis desalination: Water sources, technology, and today's challenges. *Water Res.* **2009**, *43*, 2317–2348. [CrossRef] [PubMed]
7. Pan, P.; Sun, Y.; Yuan, C.; Yan, X.; Tang, X. Research progress on ship power systems integrated with new energy sources: A review. *Renew. Sustain. Energy Rev.* **2021**, *144*, 111048. [CrossRef]
8. Ghaffour, N.; Bundschuh, J.; Mahmoudi, H.; Goosen, M.F.A. Renewable energy-driven desalination technologies: A comprehensive review on challenges and potential applications of integrated systems. *Desalination* **2015**, *356*, 94–114. [CrossRef]
9. Gude, V.G. Desalination and Sustainability—An Appraisal and Current Perspective. *Water Res.* **2016**, *89*, 87–106. [CrossRef] [PubMed]
10. Li, C.; Goswami, Y.; Stefanakos, E. Solar assisted sea water desalination: A review. *Renew. Sustain. Energy Rev.* **2013**, *19*, 136–163. [CrossRef]
11. Alrbai, M.; Enizat, J.; Hayajneh, H.; Qawasmeh, B.; Al-Dahidi, S. Energy and exergy analysis of a novel humidification-dehumidification desalination system with fogging technique. *Desalination* **2022**, *522*, 115421. [CrossRef]
12. Eder, E.; Preißinger, M. Experimental analysis of the humidification of air in bubble columns for thermal water treatment systems. *Exp. Therm. Fluid Sci.* **2020**, *115*, 110063. [CrossRef] [PubMed]
13. Sharqawy, M.H.; Al-Shalawi, I.; Antar, M.A.; Zubair, S.M. Experimental investigation of packed-bed cross-flow humidifier. *Appl. Therm. Eng.* **2017**, *117*, 584–590. [CrossRef]
14. El-Said, E.M.S.; Abdelaziz, G.B. Experimental investigation and economic assessment of a solar still performance using high-frequency ultrasound waves atomizer. *J. Clean. Prod.* **2020**, *256*, 120609. [CrossRef]
15. El-Said, E.M.S.; Dahab, M.A.; Omara, M.; Abdelaziz, G.B. Solar desalination unit coupled with a novel humidifier. *Renew. Energy* **2021**, *180*, 297–312. [CrossRef]

16. Shehata, A.I.; Kabeel, A.E.; Dawood, M.M.K.; Abo Elazm, M.M.; Abdalla, A.M.; Mehanna, A. Achievement of humidification and dehumidification desalination system by utilizing a hot water sprayer and ultrasound waves techniques. *Energy Convers. Manag.* **2019**, *201*, 112142. [CrossRef]
17. Tourab, A.; Blanco-Marigorta, A.; Elharidi, A.; Suárez López, M.J. A Novel Humidification Technique Used in Water Desalination Systems Based on the Humidification–Dehumidification Process: Experimentally and Theoretically. *Water* **2020**, *12*, 2264. [CrossRef]
18. Abed, A.H.; Hoshi, H.A.; Jabal, M.H. Experimental investigation of modified solar still coupled with high-frequency ultrasonic vaporizer and phase change material capsules. *Case Stud. Therm. Eng.* **2021**, *28*, 101531. [CrossRef]
19. Ali, E.S.; Mohammed, R.H.; Zohir, A.E.; Farid, A.M.; Elshaer, R.N.; El-Ghetany, H.H.; Askalany, A.A. Novel ultrasonic dynamic vapor sorption apparatus for adsorption drying, cooling and desalination applications. *Energy Rep.* **2022**, *8*, 8798–8804. [CrossRef]

Disclaimer/Publisher's Note: The statements, opinions and data contained in all publications are solely those of the individual author(s) and contributor(s) and not of MDPI and/or the editor(s). MDPI and/or the editor(s) disclaim responsibility for any injury to people or property resulting from any ideas, methods, instructions or products referred to in the content.